

Cite this: *Dalton Trans.*, 2021, **50**, 9310

The difference in the CO₂ adsorption capacities of different functionalized pillar-layered metal–organic frameworks (MOFs)†

Xiang-Jing Gao and He-Gen Zheng *

The excessive use of fossil energy has caused the CO₂ concentration in the atmosphere to increase year by year. MOFs are ideal CO₂ adsorbents that can be used in CO₂ capture due to their excellent characteristics. Studies of the structure–activity relationship between the small structural differences in MOFs and the CO₂ adsorption capacities are helpful for the development of efficient MOF-based CO₂ adsorbents. Therefore, a series of pillar-layered MOFs with similar structural and different functional groups were designed and synthesized. The CO₂ adsorption tests were carried out at 273 K to explore the relationship between the small structural differences in MOFs caused by different functional groups and the CO₂ adsorption capacities. Significantly, compound **6** which contains a pyridazinyl group has a 30.9% increase in CO₂ adsorption capacity compared to compound **1** with no functionalized group.

Received 14th February 2021,
Accepted 29th May 2021

DOI: 10.1039/d1dt00498k

rsc.li/dalton

Introduction

The extensive use of fossil energy has made the energy crisis and greenhouse effect increasingly serious in today's society. According to the observation data of the Mauna Loa Baseline Observatory, the average CO₂ concentration in the atmosphere in December 2019 had reached 411.79 ppm, which is a significant increase compared to 322.51 ppm in August 1969.¹ In addition to ameliorating traditional fossil energy² and developing new sustainable energy,³ the carbon capture and storage (CCS) is broadly recognised as the most economical and feasible way to reduce greenhouse gas emissions and slow down global warming in the future.⁴ Post-combustion capture, pre-combustion capture, and oxy-fuel technology are three main ways to realize CO₂ capture.⁵ Thereinto, the post-combustion capture can be technically divided into physical and chemical absorption, adsorption and membrane technologies.⁶ Chemical absorption technology is currently the most mature CO₂ capture technology, but it also faces many problems such as high energy consumption, a large amount of absorbents and equipment corrosion.⁷ Adsorption technology can effectively overcome the problems faced by chemical absorption. A

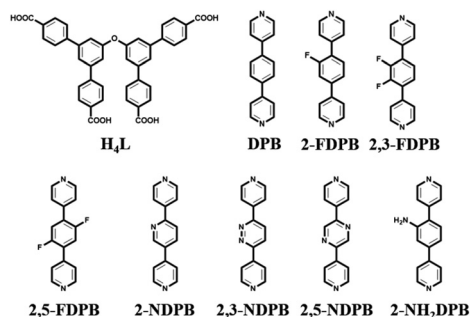
large number of porous materials, such as zeolites,⁸ activated carbon,⁹ carbon nanotubes,¹⁰ porous organic polymers¹¹ and molecular-sieves,¹² have been reported as excellent CO₂ adsorbents.

Metal–organic frameworks (MOFs) as emerging crystalline porous materials have been attracting increasing attention in recent years. Due to their designable structures, stable compositions, and permanent channels, MOFs are applied to many fields such as molecular structure determination,¹³ the adsorption and separation of substances,¹⁴ fluorescence sensing,¹⁵ catalysis,¹⁶ drug store delivery,¹⁷ *etc.*¹⁸ Compared with traditional porous materials, MOFs, whose structures can be predicted and edited by using crystal design, can be functionalized to change the structures of their channels.¹⁹ These characteristics make MOFs ideal adsorbents for CO₂.²⁰ For example, Mg-MOF-74 has a CO₂ adsorption capacity of 35.2 wt% at 296 K under 1 atm²¹ and Cu-DDQ can take up nearly 26.1 wt% of CO₂ at 296 K and 800 Torr.²² As adsorbents for CO₂, one of the important evaluation indicators is the CO₂ adsorption capacity. The CO₂ adsorption capacities of MOFs can be affected by many factors such as the pore volume,²³ characteristics of the pore,²⁴ and open metal sites.²⁵ Pillar-layered MOFs can adjust the sizes and surfaces of the channels without drastically changing the frameworks by functionalizing the pillar-ligands. Therefore, they can become an excellent platform to study the structure–activity relationship between the small structural differences in MOFs and CO₂ adsorption capacities.

Herein, a series of isostructural pillar-layered MOFs with different functional groups have been successfully designed

State Key Laboratory of Coordination Chemistry, School of Chemistry and Chemical Engineering, Collaborative Innovation Center of Advanced Microstructures, Nanjing University, Nanjing 210023, P. R. China. E-mail: zhenghg@nju.edu.cn

† Electronic supplementary information (ESI) available: IR spectra, PXRD patterns, TG diagrams, crystallographic data and other additional information of the MOFs. CCDC 2061323–2061330. For ESI and crystallographic data in CIF or other electronic format see DOI: 10.1039/d1dt00498k



Scheme 1 The structures and the corresponding abbreviations of the ligands.

and synthesized under solvothermal conditions by using $\text{Co}(\text{NO}_3)_2$, a tetra-carboxylate ligand (H_4L) and different functionalized auxiliary N-based ligands (the ligands are shown in Scheme 1). Although they have similar structures, they have different CO_2 adsorption capacities caused by their different functional groups and structural nuances. These pillar-layered MOFs can become an excellent platform for an in-depth study of the structure–activity relationship of MOFs and CO_2 adsorption capacities and help in the development of more efficient carbon capture materials based on MOFs.

Experimental

Materials and methods

All the reagents and solvents were commercially available and used without further purification. Single-crystal X-ray diffraction (SCXRD) was performed using a Bruker D8 Venture X-Ray single crystal diffractometer with graphite monochromatic $\text{Ga-K}\alpha$ radiation (λ is 1.34139 Å) as the photo-source. Infrared (IR) absorption spectra were recorded in a range of 400–4000 cm^{-1} on a Bruker Tensor II infrared spectrometer. Powder X-ray diffraction (PXRD) measurements were performed on a Bruker D8 Advance X-ray diffractometer, in which the Cu-tube was operated at 40 kV and 40 mA. Thermogravimetric analyses (TGA) were performed using a Netzche STA449F3 thermogravimetric analyser with heating from 30 °C to 600 °C under a N_2 atmosphere at a heating rate of 10 °C min^{-1} .

Synthesis

The synthesis of the ligands (H_4L and auxiliary N-based ligands) is described in the ESI.†

General procedure for the preparation of compounds 1–8: $\text{Co}(\text{NO}_3)_2 \cdot 6\text{H}_2\text{O}$ (15 mg) was dissolved in 2 mL H_2O , a mixture of H_4L (5 mg) and auxiliary N-based ligands (3 mg) (DPB for 1, 2-FDPB for 2, 2,3-FDPB for 3, 2,5-FDPB for 4, 2-NDPB for 5, 2,3-NDPB for 6, 2,5-NDPB for 7 and 2- NH_2 DPB for 8) was dissolved in 2 mL *N,N*-dimethylacetamide (DMA), and 1 ml of acetonitrile (ACN) and 50 μL HCl (1 mol L^{-1} in H_2O) were added subsequently. After being subjected to ultrasonic treatment, the mixture was sealed in a 25 mL Parr Teflon-lined

stainless steel autoclave under autogenous pressure and heated at 95 °C for 3 days. After the samples had cooled down to ambient temperature, red blocky crystals were collected and washed three times with ACN. The yields of these reactions were all around 80% (based on the auxiliary N-based ligands).

X-ray crystallography

X-ray crystallographic data of compounds 1–8 were collected at 193 K by sealing a better crystal for SCXRD in the loop with the Bruker D8 Venture X-Ray single crystal diffractometer which used ω -scan and graphite monochromatic $\text{Ga-K}\alpha$ radiation ($\lambda = 1.34139$ Å) as the photo-source. The intensity data were integrated by using the SAINT program. Empirical absorption correction was applied by using the SADABS program. The structures were solved by SHELXT and the non-hydrogen atoms were located from the trial structures and then refined anisotropically with SHELXL-2018 by using full-matrix least-squares procedures based on F^2 values.²⁶ The positions of the non-hydrogen atoms were refined with anisotropic displacement factors. The hydrogen atoms were positioned geometrically by using an idealized riding model. CCDC numbers 2061323–2061330† correspond to compounds 1–8. The crystallographic data of compounds 1–8 are listed in Tables S1 and S2.†

Results and discussion

Crystal structure description

Compounds 1–8 have isostructural frameworks with similar formulas as revealed by SCXRD. Their formulas are similar and can be expressed as $[\text{Co}_2(\text{L-H})(\text{R-DPB})_2]_n \cdot (\text{solvent})_x$, where R-DPB means DPB for 1, 2-FDPB for 2, 2,3-FDPB for 3, 2,5-FDPB for 4, 2-NDPB for 5, 2,3-NDPB for 6, 2,5-NDPB for 7 and 2- NH_2 DPB for 8. Therefore, only the structure of compound 1 will be discussed in detail as a representative for brevity. Compound 1 crystallizes in the triclinic crystal system and $P\bar{1}$ space group. There are two $\text{Co}(\text{II})$ ions, one completely deprotonated L^{4-} ligand and two auxiliary ligands (DPB) in the asymmetric unit. As shown in Fig. 1, both $\text{Co}(\text{II})$ ions are hexa-coordinated and exist in a distorted octahedral environment. They are coordinated by two nitrogen atoms from two different DPB ligands and four oxygen atoms from three different L^{4-} ligands. The carboxylic groups of L^{4-} ligands show two coordination modes: bidentate chelate coordination mode and bidentate bridge coordination mode. The Co_2^{+} ions are connected by the L^{4-} ligands to generate a two-dimensional (2D) layer (Fig. 2a). The 2D layers are connected by the DPB ligands to form a three-dimensional (3D) pillar-layered framework, which is shown in Fig. 2b. Two centrosymmetric 3D pillar-layered frameworks interpenetrate and form the final structure which has 1D square channels (~ 11 Å \times 12 Å, considering van der Waals radius) along the *b* axes (Fig. 2c).

By using the topological approach, the secondary building units (SBUs) $[\text{Co}_2(\mu\text{-COO})_2(\text{COO})_2]$ can be simplified to 6-connected nodes, and the L^{4-} ligands can be regarded as 4-con-

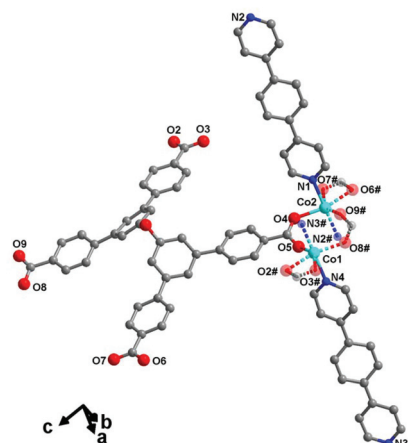


Fig. 1 The coordination environment of the binuclear Co(II); the hydrogen atoms are omitted for clarity (Gray, C; red, O; blue, N and turquoise Co).

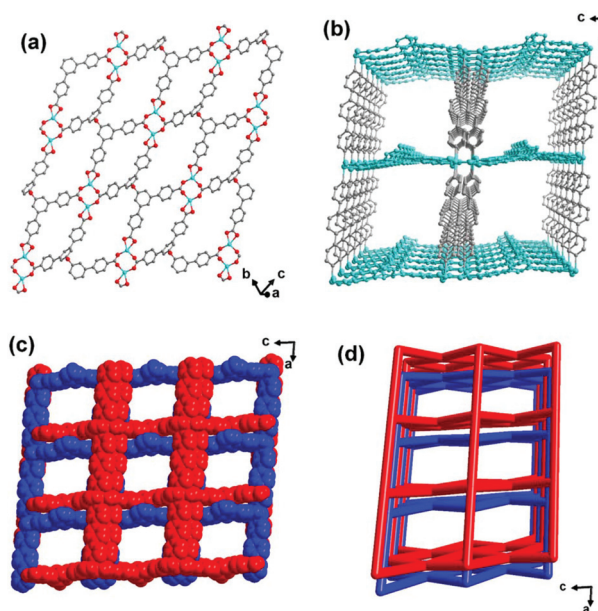


Fig. 2 (a) Perspective of the 2D layer formed by CO_2^+ ions and the L^{4-} ligands. (Gray, C; red, O and blue, N) (b) Perspective of the 3D pillar-layered framework. (The pillar-ligands appear in gray and the layer-ligands appear in turquoise.) (c) Perspective of the final 2-fold interpenetrating 3D frameworks with 1D channels along the b axis. (d) Schematic representation of the fsc topology structure in central projection mode.

nected nodes. As shown in Fig. 2d, the whole structure adopts a 2-fold interpenetrating, 4,6-connected and fsc type topology with a point symbol of $\{4^4 \cdot 6^{10} \cdot 8\}\{4^4 \cdot 6^2\}$. It contains a solvent-accessible volume of 39.1% which is calculated using the SOLV program of PLATON.²⁷

Interestingly, the L^{4-} ligands show disorder in compounds 2–4, 6 and 8. This disordered structure leads to lower calculated solvent-accessible volume and smaller channels (Fig. 3), which may further affect the CO_2 adsorption capacities.

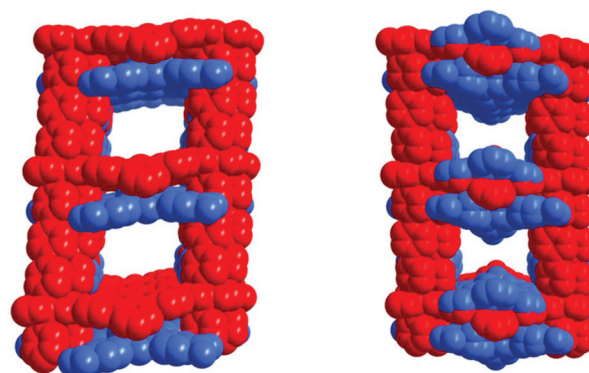


Fig. 3 The schematic diagrams of the ordered 2-fold interpenetrating 3D frameworks in compound 1, 5 and 7 (left) and the disordered 2-fold interpenetrating 3D frameworks in compound 2–4, 6 and 8 (right).

Characterization

A series of characterization tests such as IR absorption, PXRD, and TGA were conducted on the as-synthesized and activated compounds 1–8 before the CO_2 adsorption tests.

IR absorption. As shown in Fig. S1,[†] the strong peaks around 1605 cm^{-1} and 1410 cm^{-1} for 1–8 are associated with the asymmetric and symmetric stretching vibrations of the coordinated carboxylate group COO^- . The asymmetric and symmetric stretching vibrations of the N–H bond can be observed at 3333 cm^{-1} and 3225 cm^{-1} in compound 8.

PXRD. The PXRD patterns are given in Fig. S2[†] to confirm the purities of compounds 1–8 which are synthesized by the solvothermal method. The experimental PXRD patterns before activation and the simulated PXRD patterns match perfectly, which indicates that the as-synthesized compounds are in pure phase. Before the CO_2 adsorption tests, these compounds are activated by soaking them in ACN for three days and then vacuum-drying at $40\text{ }^\circ\text{C}$ for 2 hours. The experimental PXRD patterns after activation also match perfectly with the simulated PXRD patterns, which indicates that the activation process does not destroy the structure and the channels of these MOFs are permanent.

TGA. In order to characterize the thermal stability of the as-synthesized compounds and the residual solvent content of the activated compounds, their thermal behaviours are measured by using TG analysis (Fig. S3[†]). For the as-synthesized samples before activation, a weight loss before reaching $280\text{ }^\circ\text{C}$ can be attributed to the release of solvent molecules and all the frameworks remain stable until $320\text{ }^\circ\text{C}$. Higher thermal destruction temperatures of these as-synthesized compounds show that they have good thermal stability. As for the activated samples, most of them (except 6 and 8) do not show obvious weight loss until $340\text{ }^\circ\text{C}$, which indicates that there is almost no residual solvent in the frameworks of compounds 6 and 8 after activation. It is worth noting that these solvent molecules, most likely water molecules, maybe have

some impact on the CO₂ adsorption capacities. Most of the activated samples (except 2 and 3) have higher thermal destruction temperatures than the non-activated samples. This phenomenon may be due to the interaction between the high boiling point solvent in the non-activated sample and the frameworks during heating, which makes the frameworks more prone to collapse. In summary, the activated samples have better thermal stability than the non-activated samples and almost little residual solvent. The weight loss percentage, weight loss temperature range and thermal destruction temperature are listed in Table S3.†

CO₂ adsorption

Low-pressure CO₂ adsorption capacities are measured at 273 K. The reversible isotherms are shown in Fig. 4. Compound 1, whose pillar-ligand is not modified by any functional groups, can adsorb 70.0 cm³ g⁻¹ CO₂ at 273 K and 850 mmHg. Comparatively, the CO₂ adsorption capacity of compound 2, whose pillar-ligand is modified by a fluorine atom, is slightly increased. It can adsorb 74.9 cm³ g⁻¹ CO₂ under the same experimental conditions. However, compounds 3 and 4, whose pillar-ligands are modified by two fluorine atoms at the *ortho*-position and the *para*-position respectively, do not have an obvious increase in CO₂ adsorption capacities when compared

with 1. These phenomena prove that fluorine atoms are not very good CO₂ adsorption active sites. From the perspective of crystal structures, these three compounds 2–4 modified with fluorine atoms have similar porosities, structural disorder and poor adsorption active sites. Interestingly, the CO₂ adsorption capacities of compounds 3 and 4 are slightly decreased when compared with that of 2. This is probably because the larger fluorine atoms cause a decrease in solvent-accessible volume.

There are bigger differences in the CO₂ adsorption capacities of compounds 5–7 whose pillar-ligand is modified by nitrogen atoms. Compounds 1 and 5 have similar solvent-accessible volume and they do not have disorder in their structures. However, one of the carbon atoms in the middle phenyl group of the ligand is replaced by one nitrogen atom when comparing 2-NDPB ligands with non-functionalized DPB ligands. This difference increases the polarity of the pillar-ligands in compound 5, which leads to the stronger interaction between the pillar-ligands and the CO₂ molecules. So the CO₂ adsorption capacity of compound 5 is slightly higher than that of compound 1. Compound 7 also has a similar solvent-accessible volume and ordered structure to 1. Two carbon atoms at the *para*-position in the middle phenyl group of the ligand are replaced by two nitrogen atoms when comparing 2,5-NDPB ligands with non-functionalized DPB ligands. However, its CO₂

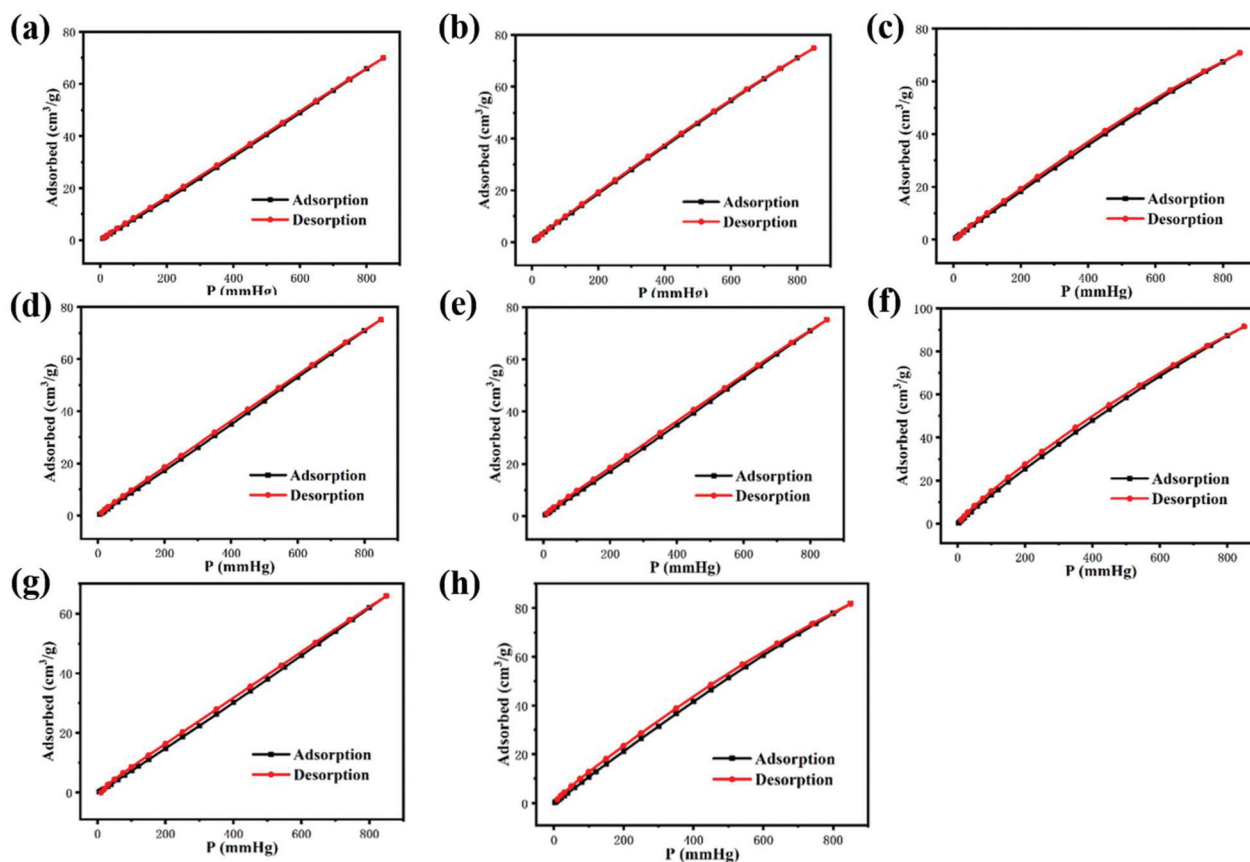


Fig. 4 Low-pressure CO₂ adsorption (black square) and desorption (red circle) isotherms of compound 1 (a), 2 (b), 3 (c), 4 (d), 5 (e), 6 (f), 7 (g), and 8 (h) at 273 K.

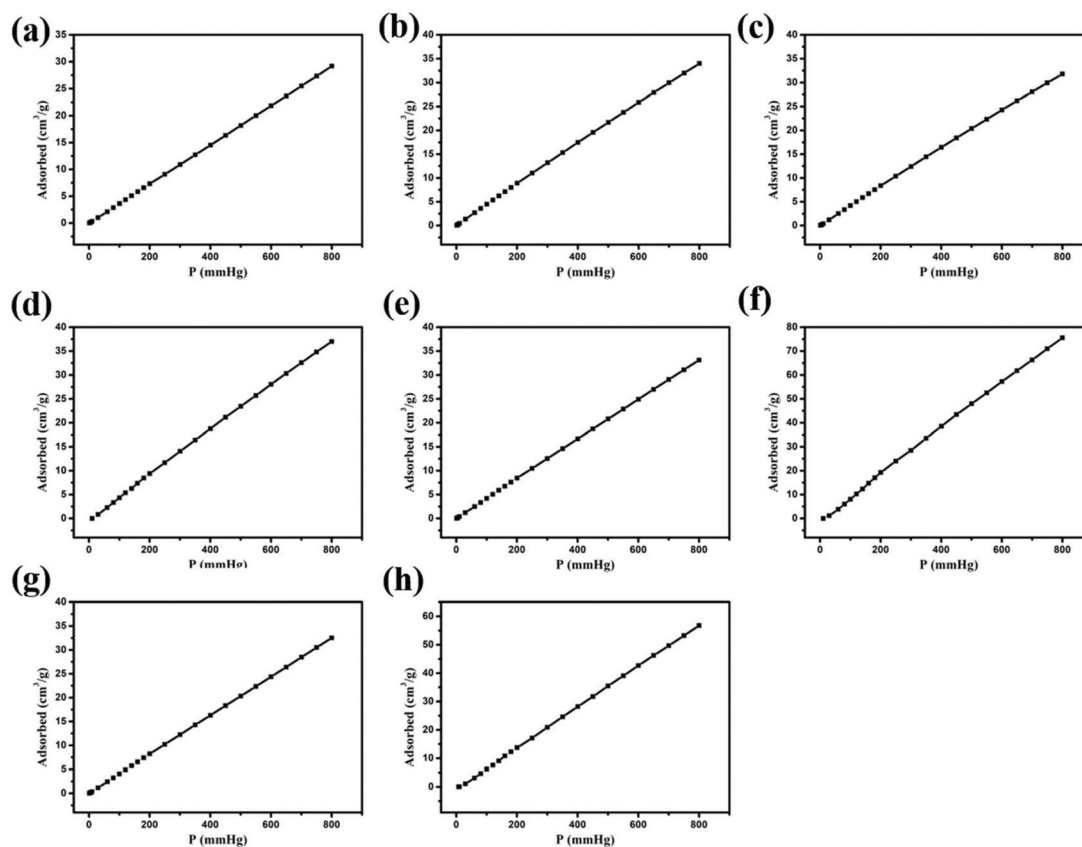


Fig. 5 Low-pressure CO₂ adsorption isotherms of compounds 1 (a), 2 (b), 3 (c), 4 (d), 5 (e), 6 (f), 7 (g), and 8 (h) at 298 K.

adsorption capacity is lower than that of **1** and even lower than that of **5**. From the perspective of crystal structures, the dihedral angles between the phenyl rings and the pyridyl rings in **7** are smaller than those in **1** and **5** as shown in Table S4.† The better coplanar 2,5-NDPB ligands are more symmetrical than DPB and 2-NDPB which leads to a decrease in the CO₂ adsorption capacity of compound **7**. In contrast, compound **6** has a disordered structure which leads to lower calculated solvent-accessible volume and smaller channels. Two carbon atoms at the *ortho*-position in the middle phenyl group of the ligand are replaced by two nitrogen atoms when comparing 2,3-NDPB ligands with non-functionalized DPB ligands. Compared with other ligands, significant bending of the 2,3-NDPB ligands in compound **6** can be revealed by SCXRD as shown in Fig. S4.† Therefore, the symmetry of the 2,3-NDPB ligands decreased significantly when comparing with other ligands. The pillar-ligands with low symmetry are more polar and have a stronger interaction with CO₂ molecules. So, among these pillar-layered compounds, compound **6** has the largest adsorption capacities (91.6 cm³ g⁻¹ at 273 K and 850 mmHg).

Compound **8** has the pillar-ligand based on aniline and can adsorb 81.7 cm³ g⁻¹ CO₂ at 273 K and 850 mmHg, which is much higher than that of compound **1** with no functionalized group because the 2-NH₂DPB ligand is alkaline and has strong interactions with acidic CO₂ molecules.

The CO₂ adsorption tests are repeated twice to verify whether the CO₂ adsorption capacities of compounds **1–8** are repeatable. As shown in Fig. S5,† the CO₂ adsorption isotherms of the two tests are almost the same.

Compounds **1–8** show similar adsorption behaviour at 298 K to that at 273 K, except for the decrease in adsorption capacity. As shown in Fig. 5, compounds **6** and **8** maintain higher CO₂ adsorption capacities at 298 K than others due to the interaction between the residual solvent and CO₂ molecules (75.6 and 56.8 cm³ g⁻¹, respectively, at 298 K and 850 mmHg).

The parameters that may affect the CO₂ adsorption capacities, the specific adsorption capacities and the isosteric heats of adsorption (Q_{st}) of compounds **1–8** are listed in Table S4.† As shown in Fig. S6 and S7,† the Q_{st} of compounds **1–8** are comparable to those of other MOF materials reported in other literature.

Table S5† depicts the CO₂ adsorption performance of some MOFs mentioned in other reports. According to the results, the CO₂ adsorption capacities of compounds **1–8** are similar to the values for some other MOF materials.

Conclusions

In summary, we have designed and synthesized a series of pillar-layered MOFs with similar structures *via* the solvo-

thermal method by using $\text{Co}(\text{NO}_3)_2$, a tetra-carboxylate ligand (H_4L) and N-based pillar-ligands with different functional groups. They are all 2-fold interpenetrating 3D frameworks with 1D channels along the b axis. All the frameworks remain stable after being activated by soaking them in ACN for three days and then vacuum-drying at 40 °C for 2 hours. Then, low-pressure CO_2 adsorption tests are carried out at 273 K to explore the effect of different functional groups on the CO_2 adsorption capacities. Significantly, compound **6** which contains a pyridazinyl group has a 30.9% increase in CO_2 adsorption capacity compared to compound **1** with no functionalized group. This work can help in the development of new and efficient MOF-based CO_2 adsorbents that can be used in CCS and solve the problem of the greenhouse effect.

Conflicts of interest

There are no conflicts to declare.

Acknowledgements

This work was financially supported by the grants from the National Natural Science Foundation of China (21771101).

References

- ESRL, *Trends in atmospheric carbon dioxide, ESRL's global monitoring division*, 2020.
- Z. Zhang, Z. Zhu, B. Shen and L. Liu, *Energy*, 2019, **171**, 581; M. M. Hasana and M. M. Rahmana, *Renewable Sustainable Energy Rev.*, 2017, **74**, 938; M. Ao, G. H. Pham, J. Sunarso, M. O. Tade and S. Liu, *ACS Catal.*, 2018, **8**, 7025.
- S. Chu, Y. Cui and N. Liu, *Nat. Mater.*, 2017, **16**, 16; J. H. Montoya, L. C. Seitz, P. Chakthranont, A. Vojvodic, T. F. Jaramillo and J. K. Nørskov, *Nat. Mater.*, 2017, **16**, 70.
- N. Mac Dowell, N. Florin, A. Buchard, J. Hallett, A. Galindo, G. Jackson, C. S. Adjiman, C. K. Williams, N. Shah and P. Fennell, *Energy Environ. Sci.*, 2010, **3**, 1645; M. E. Boot-Handford, J. C. Abanades, E. J. Anthony, M. J. Blunt, S. Brandani, N. Mac Dowell, J. R. Fernández, M.-C. Ferrari, R. Gross, J. P. Hallett, R. S. Haszeldine, P. Heptonstall, A. Lyngfelt, Z. Makuch, E. Mangano, R. T. J. Porter, M. Pourkashanian, G. T. Rochelle, N. Shah, J. G. Yao and P. S. Fennell, *Energy Environ. Sci.*, 2014, **7**, 130; M. Bui, C. S. Adjiman, A. Bardow, E. J. Anthony, A. Boston, S. Brown, P. S. Fennell, S. Fuss, A. Galindo, L. A. Hackett, J. P. Hallett, H. J. Herzog, G. Jackson, J. Kemper, S. Krevor, G. C. Maitland, M. Matuszewski, I. S. Metcalfe, C. Petit, G. Puxty, J. Reimer, D. M. Reiner, E. S. Rubin, S. A. Scott, N. Shah, B. Smit, J. P. M. Trusler, P. Webley, J. Wilcox and N. M. Dowell, *Energy Environ. Sci.*, 2018, **11**, 1062.
- R. Notz, I. Tönnies, N. McCann, G. Scheffknecht and H. Hasse, *Chem. Ing. Tech.*, 2010, **82**, 1639.
- T. Ghanbari, F. Abnisa and W. M. A. Wan Daud, *Sci. Total Environ.*, 2020, **707**, 135090.
- C.-H. Yu, C.-H. Huang and C.-S. Tan, *Aerosol Air Qual. Res.*, 2012, **12**, 745.
- S. J. Chen, M. Zhu, Y. Fu, Y. X. Huang, Z. C. Tao and W. L. Li, *Appl. Energy*, 2017, **191**, 87; V. Garshasbi, M. Jahangiri and M. Anbia, *Appl. Surf. Sci.*, 2017, **393**, 225; S. Krachumram, K. C. Chanapattharapol and N. Kamonsutthipajit, *Microporous Mesoporous Mater.*, 2021, **310**, 110632; S. Kumar, R. Srivastava and J. Koh, *J. CO₂ Util.*, 2020, **41**, 101251; C. Megías-Sayago, R. Bingre, L. Huang, G. Lutzweiler, Q. Wang and B. Louis, *Front. Chem.*, 2019, **7**, 551.
- Y.-C. Chiang, C.-Y. Yeh and C.-H. Weng, *Appl. Sci.*, 2019, **9**, 1977; Y. Boyjoo, Y. Chen, H. Zhong, H. Tian, J. Pan, V. K. Pareek, S. P. Jiang, J.-F. Lamonier, M. Jaroniec and J. Liu, *Carbon*, 2017, **116**, 490; G. Singh, I. Y. Kim, K. S. Lakhi, P. Srivastava, R. Naidu and A. Vinu, *Carbon*, 2017, **116**, 448; A. Mukherjee, J. A. Okolie, A. Abdelrasoul, C. Niu and A. K. Dalai, *J. Environ. Sci.*, 2019, **83**, 46.
- N. Hsan, P. K. Dutta, S. Kumar, N. Das and J. Koh, *J. CO₂ Util.*, 2020, **41**, 101237; B. Liu, L. Ye, R. Wang, J. Yang, Y. Zhang, R. Guan, L. Tian and X. Chen, *ACS Appl. Mater. Interfaces*, 2018, **10**, 4001; L. Keller, B. Ohs, J. Lenhart, L. Abduly, P. Blanke and M. Wessling, *Carbon*, 2018, **126**, 338; R. R. Haikal, A. B. Soliman, M. Amin, S. G. Karakalos, Y. S. Hassan, A. M. Elmansi, I. H. Hafez, M. R. Berber, A. Hassanien and M. H. Alkordi, *Appl. Catal., B*, 2017, **207**, 347; M. Irani, A. T. Jacobson, K. A. M. Gasem and M. Fan, *Fuel*, 2017, **206**, 10.
- M. M. Abdelnaby, A. M. Alloush, N. A. A. Qasem, B. A. Al-Maythaly, R. B. Mansour, K. E. Cordova and O. C. S. Al Hamouz, *J. Mater. Chem. A*, 2018, **6**, 6455; M. M. Abdelnaby, K. E. Cordova, I. Abdulazeez, A. M. Alloush, B. A. Al-Maythaly, Y. Mankour, K. Alhooshani, T. A. Saleh and O. C. S. Al Hamouz, *ACS Appl. Mater. Interfaces*, 2020, **12**, 47984.
- G. Zhang, P. Zhao, L. Hao, Y. Xu and H. Cheng, *Sep. Purif. Technol.*, 2019, **209**, 516; M. Jiang, B. Li, X. Cui, Q. Yang, Z. Bao, Y. Yang, H. Wu, W. Zhou, B. Chen and H. Xing, *ACS Appl. Mater. Interfaces*, 2018, **10**, 16628.
- S. Lee, E. A. Kapustin and O. M. Yaghi, *Science*, 2016, **353**, 808; X. Pei, H.-B. Bürgi, E. A. Kapustin, Y. Liu and O. M. Yaghi, *J. Am. Chem. Soc.*, 2019, **141**, 18862; M. Mon, R. Bruno, S. Sanz-Navarro, C. Negro, J. Ferrando-Soria, L. Bartella, L. D. Donna, M. Prejanò, T. Marino, A. Leyva-Pérez, D. Armentano and E. Pardo, *Nat. Commun.*, 2020, **11**, 3080.
- S. Zhang, R. Ou, H. Ma, J. Lu, M. M. B. Holl and H. Wang, *Chem. Eng. J.*, 2021, **405**, 127037; L. Xing, J. Liu, T. Qi, L. Wang, Z. Wang and S. Zhang, *Appl. Catal., B*, 2020, **275**, 119143; L. Liu, Z. Yao, Y. Ye, Y. Yang, Q. Lin, Z. Zhang, M. O'Keeffe and S. Xiang, *J. Am. Chem. Soc.*, 2020, **142**, 9258; Y. Zhao, Y. Wei, L. Lyu, Q. Hou, J. Caro and H. Wang, *J. Am. Chem. Soc.*, 2020, **142**, 20915; Y. Chen, X. Zhang, M. R. Mian, F. A. Son, K. Zhang, R. Cao, Z. Chen, S.-J. Lee,

- K. B. Idrees, T. A. Goetjen, J. Lyu, P. Li, Q. Xia, Z. Li, J. T. Hupp, T. Islamoglu, A. Napolitano, G. W. Peterson and O. K. Farha, *J. Am. Chem. Soc.*, 2020, **142**, 21428; X. Gao, G. Sun, F. Ge and H. Zheng, *Inorg. Chem.*, 2019, **58**, 8396.
- 15 T.-Y. Luo, P. Das, D. L. White, C. Liu, A. Star and N. L. Rosi, *J. Am. Chem. Soc.*, 2020, **142**, 2897; J. Dong, P. Shen, S. Ying, Z.-J. Li, Y. D. Yuan, Y. Wang, X. Zheng, S. B. Peh, H. Yuan, G. Liu, Y. Cheng, Y. Pan, L. Shi, J. Zhang, D. Yuan, B. Liu, Z. Zhao, B. Z. Tang and D. Zhao, *Chem. Mater.*, 2020, **32**, 6706; X.-L. Yang, C. Ding, R.-F. Guan, W.-H. Zhang, Y. Feng and M.-H. Xie, *J. Hazard. Mater.*, 2021, **403**, 123698.
- 16 Z. Xue, Y. Li, Y. Zhang, W. Geng, B. Jia, J. Tang, S. Bao, H.-P. Wang, Y. Fan, Z. Wei, Z. Zhang, Z. Ke, G. Li and C.-Y. Su, *Adv. Energy Mater.*, 2018, **8**, 1801564; L. Jiao, Y. Wang, H.-L. Jiang and Q. Xu, *Adv. Mater.*, 2018, **30**, 1703663; J.-D. Xiao and H.-L. Jiang, *Acc. Chem. Res.*, 2019, **52**, 356; G.-Y. Qiao, S. Yuan, J. Pang, H. Rao, C. T. Lollar, D. Dang, J.-S. Qin, H.-C. Zhou and J. Yu, *Angew. Chem., Int. Ed.*, 2020, **59**, 18224.
- 17 H. Li, N. Lv, X. Li, B. Liu, J. Feng, X. Ren, T. Guo, D. Chen, J. F. Stoddart, R. Gref and J. Zhang, *Nanoscale*, 2017, **9**, 7454; W. Cai, J. Wang, C. Chu, W. Chen, C. Wu and G. Liu, *Adv. Sci.*, 2019, **6**, 1801526; B.-T. Liu, X.-H. Pan, D.-Y. Nie, X.-J. Hu, E.-P. Liu and T.-F. Liu, *Adv. Mater.*, 2020, **32**, 2005912; H. Wang, L. Han, D. Zheng, M. Yang, Y. H. Andaloussi, P. Cheng, Z. Zhang, S. Ma, M. J. Zaworotko, Y. Feng and Y. Chen, *Angew. Chem., Int. Ed.*, 2020, **59**, 6263.
- 18 X. Ma, Z. Deng, Z. Li, D. Chen, X. Wan, X. Wang and X. Peng, *J. Mater. Chem. A*, 2020, **8**, 22728; S. E. Gilson, M. Fairley, P. Julien, A. G. Oliver, S. L. Hanna, G. Arntz, O. K. Farha, J. A. LaVerne and P. C. Burns, *J. Am. Chem. Soc.*, 2020, **142**, 13299; M. K. Sarango-Ramírez, D.-W. Lim, D. I. Kolokolov, A. E. Khudozhnikov, A. G. Stepanov and H. Kitagawa, *J. Am. Chem. Soc.*, 2020, **142**, 6861.
- 19 S. Henke, A. Schneemann and R. A. Fischer, *Adv. Funct. Mater.*, 2013, **23**, 5990; Z. Shao, C. Huang, J. Dang, Q. Wu, Y. Liu, J. Ding and H. Hou, *Chem. Mater.*, 2018, **30**, 7979; A. Kirchon, L. Feng, H. F. Drake, E. A. Josepha and H.-C. Zhou, *Chem. Soc. Rev.*, 2018, **47**, 8611.
- 20 C. A. Trickett, A. Helal, B. A. Al-Maythaly, Z. H. Yamani, K. E. Cordova and O. M. Yaghi, *Nat. Rev. Mater.*, 2017, **2**, 17045.
- 21 S. R. Caskey, A. G. Wong-Foy and A. J. Matzger, *J. Am. Chem. Soc.*, 2008, **130**, 10870.
- 22 Y. Zhu, Y.-M. Wang, S.-Y. Zhao, P. Liu, C. Wei, Y.-L. Wu, C.-K. Xia and J.-M. Xie, *Inorg. Chem.*, 2014, **53**, 7692.
- 23 Y. Lin, C. Kong, Q. Zhang and L. Chen, *Adv. Energy Mater.*, 2017, **7**, 1601296.
- 24 E. J. Kim, R. L. Siegelman, H. Z. H. Jiang, A. C. Forse, J.-H. Lee, J. D. Martell, P. J. Milner, J. M. Falkowski, J. B. Neaton, J. A. Reimer, S. C. Weston and J. R. Long, *Science*, 2020, **369**, 392; G. Zhang, G. Wei, Z. Liu, S. R. J. Oliver and H. Fei, *Chem. Mater.*, 2016, **28**, 6276; G. Xu, Z. Meng, X. Guo, H. Zhu, K. Deng, C. Xiao and Y. Liu, *Comput. Mater. Sci.*, 2019, **168**, 58; Z. Zhang, Q. Ding, J. Cui, X. Cui and H. Xing, *Sci. China Mater.*, 2021, **64**, 691; D. K. Yoo, T.-U. Yoon, Y.-S. Bae and S. H. Jhung, *Chem. Eng. J.*, 2020, **380**, 122496.
- 25 H.-H. Wang, L. Hou, Y.-Z. Li, C.-Y. Jiang, Y.-Y. Wang and Z. Zhu, *ACS Appl. Mater. Interfaces*, 2017, **9**, 17969; L. Kan, L. Li, G. Li, L. Zhang and Y. Liu, *Inorg. Chem. Front.*, 2020, **7**, 731.
- 26 G. M. Sheldrick, *Acta Crystallogr., Sect. A: Found. Adv.*, 2015, **71**, 3; G. M. Sheldrick, *Acta Crystallogr., Sect. C: Struct. Chem.*, 2015, **71**, 3.
- 27 A. L. Spek, *J. Appl. Crystallogr.*, 2003, **36**, 7.